Nanoscale

Accepted Manuscript

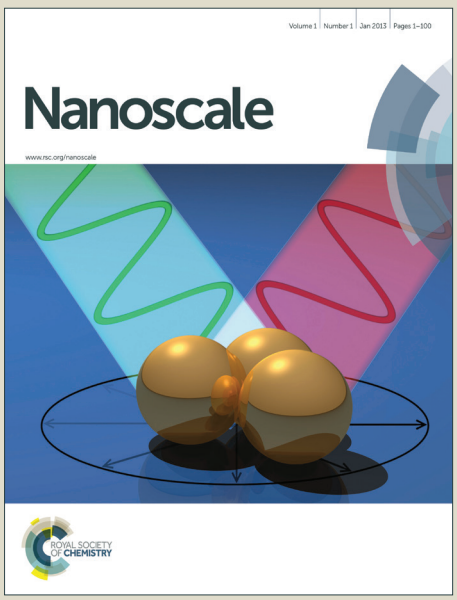

ROYAL SOCIETY OF CHEMISTRY

www.rsc.org/nanoscale

Nanoscale

RSCPublishing

COMMUNICATION

From gold porphyrin to gold nanoparticles: catalytic nanomaterials for glucose oxidation

Cite this: DOI: 10.1039/x0xx00000x

Kamal Elouarzaki[a], Alan Le Goff[a], Michael Holzinger[a], Charles Agnès[b], Florence Duclairoir[b], Jean-Luc Putaux[c] and Serge Cosnier[a]*

Received 00th January 2012,
Accepted 00th January 2012

DOI: 10.1039/x0xx00000x

www.rsc.org/

Au(III) porphyrin was synthesized and evaluated for electrocatalytic oxidation of glucose. These Au(III) porphyrin, immobilized on a multiwalled carbon nanotube matrix, oxidized glucose at low overpotentials. Furthermore, AuNPs were electrogenerated by reduction of the Au(III) porphyrins. The electrocatalytic properties towards glucose oxidation of these compounds were compared and characterized with electron microscopy and XPS.

Electrocatalytic glucose oxidation is currently of widespread interest because of its application in glucose biosensors and glucose fuel cells[1–3]. Due to the high cost and limited supply of noble metals such as platinum and the instability and fragility of redox enzymes such as glucose oxidases or dehydrogenases[3,4], molecular abiotic or bioinspired catalysts providing sufficient catalytic activity represent a promising alternative. Platinum or gold electrodes[5], as well as redox enzymes, are well described for the oxidation of glucose. Gold nanoparticles (AuNPs) have also been studied extensively for electrocatalytic oxidation of glucose[6–8]. However, only few molecular catalysts show interesting catalytic properties towards the oxidation of glucose[9,10]. Porphyrin complexes of gold(III) gained particular interest due to their promising properties as chemotherapeutics against tumour cells[11–13], Human Immunodeficiency Virus[14], and as chromophores in photophysical molecular systems[15–18]. Even if metal porphyrins are well known for many applications in catalysis or electrocatalysis, only few reactions such as the cycloisomerization of allenones can be catalyzed by gold(III) porphyrins[19]. In addition, gold(III) porphyrins are mainly insoluble in water and their electrochemical properties in water were scarcely studied. In this context, Kadish et al. studied the Au(III)/Au(II) reduction process of gold(III) porphyrins in organic media[16,20,21]. Here, we present fundamental investigation of the reduction process of gold(III) porphyrin in organic media and demonstrate, for the first time, its role as electrocatalyst of the oxidation of glucose in aqueous media.

We employed a simple method for the evaluation of the electrocatalytic activity of these water-insoluble porphyrin compounds by immobilization of the catalyst on multiwalled carbon nanotubes (MWCNTs). The use of MWCNT support allows improving the catalytic properties of supported catalysts due to the enormous specific surface area, unique electrical or electrochemical properties, and their ability to easily adsorb π–extended molecules [10,22,23]. The electrocatalytic activity of deuteroporphyrin IX dimethyl ester gold(III) (DPDE)Au(III)), immobilized on MWCNT electrodes, was studied towards glucose oxidation. Furthermore, it was evidenced that the electrochemical reduction of (DPDE)Au(III) initiates the formation of AuNPs. These gold-based MWCNT electrodes were characterized using electrochemical methods, electron microscopy, and XPS. Both gold compounds (Au(III) and Au(0)) and their respective electrocatalytic properties towards glucose oxidation in alkaline medium were compared.

Cyclic voltammograms of deuteroporphyrin IX dimethyl ester (H_2(DPDE))and (DPDE)Au(III) in DMF are illustrated in Figure 1A. Two one-electron reduction waves at $E_{1/2}$= -1.65 V and -2.05 V (vs. Ag/Ag^+) are observed for H_2(DPDE) which is consistent with the stepwise formation of a porphyrin π–anion radical followed by the dianion formation. (DPDE)Au(III) exhibits two reduction features, one reduction processes correspond to the porphyrin ligand at $E_{1/2}$= -1.65 V (vs. Ag/Ag^+), and the reduction wave observed at $E_{1/2}$= -1.12 V (vs. Ag/Ag^+) corresponds to the Au(III)/Au(II) redox couple. As reported by Kadish et al, porphyrin gold(III) undergoes monoelectronic reduction to give a gold(II) porphyrin according to spectroelectrochemical and electron spin resonance studies[20]. (DPDE)Au(III)-functionalized MWCNT electrodes were obtained by deposition of a catalyst-MWCNT mixture as an ink on glassy carbon electrode (Figure 1B). The ink was formed by using ultrasound for 30 min of a mixture of MWCNTs, (DPDE)Au(III) and Nafion in NMP. Figure 1C displays the electrochemical behaviour of MWCNT/(DPDE)Au(III) electrodes in DMF.

Two reversible one-electron redox system are observed at $E_{1/2}$ = -1.27 V (vs. Ag/Ag^+) and $E_{1/2}$ = -1.68 V (vs. Ag/Ag^+) representing the reduction of Au (III) to Au (II) porphyrin and the formation of the π-anion radical, respectively. The peak separations were virtually zero and the full widths at half maximum (E_{p1} = 98 mV, E_{p2}= 110 mV, (vs. Ag/Ag^+) both at 20 mV s^{-1}) are close to the theoretical value of 90 mV for a redox system involving one electron. By integration of the charge under the Au(III)/Au(II) oxidation or reduction peak, a surface

concentration of 4.4 10^{-9} mol cm^{-2} could be determined, corresponding to 13 monolayers of closely-packed porphyrin metal complexes. These results confirm the immobilization of the gold complex on MWCNTs with high surface coverage and excellent electron transfer rates between adsorbed (DPDE)Au(III) and MWCNTs.

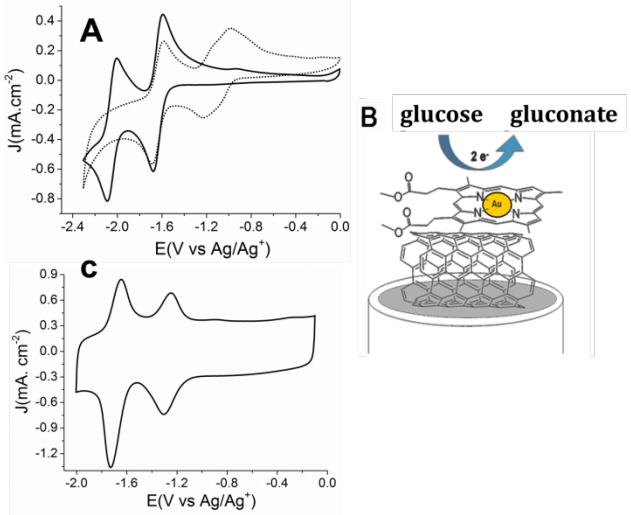

Figure 1. (A) Cyclic voltammograms of a 1 mmol L^{-1} solution of (DPDE)Au(III)(dashed line) and H_2(DPDE) at 100 mV s^{-1} (black line); (B) Schematic representation of the MWCNT/(DPDE)Au(III) electrode (C) Cyclic voltammetry of MWCNT/(DPDE)Au(III) electrode at 20 mV s^{-1}. The measurements were performed in DMF.

Figure 2A shows the cyclic voltammograms of a MWCNT/(DPDE)Au(III) electrode in absence (a) and presence(b, c and d) of different concentrations of glucose. Upon addition of glucose, the oxidation current drastically increased with an onset potential of ca. -0.46 V (vs. SCE). In addition, catalytic current increases linearly with the glucose concentration.

The anodic catalytic wave exhibits a twisted shape, i.e., a catalytic current decrease at higher overpotentials followed by current recovery upon reversed scan. This behaviour corresponds to an electrocatalytic deactivation of (DPDE)Au(III) occurring at increasing overpotentials. On the reverse scan, catalytic current is recovered by reductive regeneration of the catalyst. This mechanism was already observed for certain redox enzymes[24] and metal electrodes[5]. Furthermore, this oxidative activation/reductive deactivation mechanism has intensively been studied for a similar Rh(III) complex[10]. This behaviour is caused by formation of a metal-hydroxo/alkoxo derivative. In case of electrocatalytic glucose oxidation by (DPDE)Au(III), a similar gold hydroxide specie is likely involved in the deactivation process as encountered for both the Rh(III) complex[10] and Au(0) metal electrodes[5].

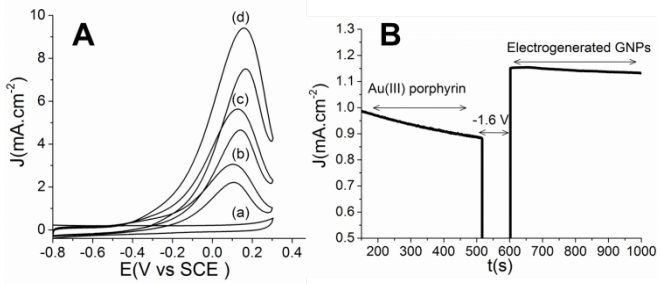

Figure 2. (A) Cyclic voltammograms of MWCNT/(DPDE) Au(III) electrodes at a scan rate of 50 mV s^{-1} in presence of (a) 0 mM, (b) 250 mM, (c) 500 mM and (d) 1 M glucose (Measurements were performed in KOH solution (pH=13) solution under nitrogen atmosphere at 20 °C ; (B) Chronoamperometric measurements of MWCNT/(DPDE)Au(III) electrodes obtained at 0.15 V before and after poising the electrode at -1.6 V. The measurements were performed in 1 M of glucose under nitrogen atmosphere (supporting electrolyte: KOH solution, pH=13).

This deactivation process was also confirmed by chronoamperometric measurements (Figure 2B). It appears that the initial anodic current intensity (1 mA cm^{-2}) recorded at 0.15 V, corresponding to the top of the catalytic peak, decreases continuously over time, namely -13 % after 500 s. A similar behaviour was observed for the MWCNT/(DPDE)Au(III) electrode previously reduced at -1.6 V (vs. SCE). The latter, however, exhibits a slightly higher initial catalytic current and a relative better stability than MWCNT/(DPDE)Au(III) electrode. It is well known that glucose can induce the conversion of Au(III) salts into Au(0)[25]. In addition, MWCNT/(DPDE)Au(III) electrodes exhibit an irreversible reduction at -1.6 V (vs. SCE). To investigate the possible formation of gold nanoparticles from (DPDE)Au(III), we studied the stability of MWCNT/(DPDE)Au(III) upon reduction or in the presence of glucose. Figure 3 shows the comparison between the electroactivity of MWCNT/(DPDE)Au(III) electrode, MWCNT/(DPDE)Au(III) electrode previously poised for several seconds at -1.6 V (vs. SCE) and MWCNT/$HAuCl_4$ electrode (commercial $HAuCl_4$ salt is replaced by (DPDE)Au(III) in the catalyst ink).

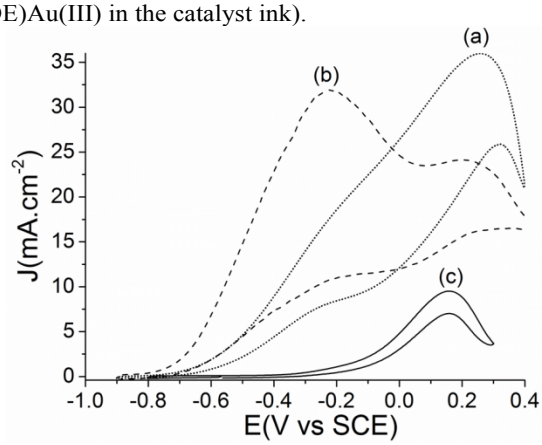

Figure 3. Cyclic voltammograms of (a) MWCNT/(DPDE)Au(III) after poising the electrode at -1.6 V, (b) MWCNT/$HAuCl_4$ and (c) MWCNT/(DPDE)Au(III) electrodes. The measurements were performed in 1 M of glucose obtained at 20 mV s^{-1} under nitrogen atmosphere (supporting electrolyte: KOH solution, pH =13).

Electrooxidation toward glucose was carried out in aqueous solution containing potassium hydroxide (pH 13) and 1 mol L^{-1} glucose, using cyclic voltammetry measurements, sweeping from −0.9 V (vs. SCE) to 0.35 V (vs. SCE) at a scan rate of 20 mV s^{-1}. Commercial $HAuCl_4$ is rapidly reduced by glucose to Au(0). This is confirmed by the electrocatalytic Au(0) signature[5] which is characterized by two well-defined current peaks with an onset potential of E = -0.78 V (vs. SCE). This is commonly observed for the electrocatalytic oxidation of glucose by Au(0) electrodes. A similar signature is also observed for MWCNT/(DPDE)Au(III) electrode previously poised at -1.6 V (vs. SCE). This behavior indicates that (DPDE)Au(III) is only reduced to Au(0) at negative potentials below -1.6 V (vs. SCE). In this case, similar Au(0) response between $HAuCl_4$ and (DPDE)Au(III) confirms the respective formation of Au(0) from respective reduction of $HAuCl_4$ by glucose and reduction of (DPDE)Au(III) by electrolysis at -1.6 V (vs. SCE).

When comparing Au(0) and (DPDE)Au(III), the first oxidation peak observed at -0.3 V (vs. SCE) at Au(0) electrode is inexistent in case of (DPDE)Au(III). The second oxidation peak around 0.25 V (vs. SCE) is observed for both catalysts, Au(0) and (DPDE)Au(III). The first oxidation peak involves electrosorption and dehydrogenation of glucose on gold electrode. The second peak exhibits similar shape with both Au(0) and (DPDE)Au(III) electrodes, which might be due to the occurrence of a similar mechanism for both gold-based electrode, i. e., the oxidation of gold-gluconolactone intermediate. The inexistent electrosorption mechanism on (DPDE)Au(III) is likely caused by the occurrence of a molecular CE mechanism[26], i. e., chemical dehydrogenation mechanism upon glucose binding followed by electron transfer. This mechanism was already proposed for the (DPDE)Rh(III) catalyst[10]. Chronoamperometric measurements were performed to estimate the catalyst efficiency. By taking into account the (DPDE)Au(III) surface of 4.4 10^{-9} mol cm^{-2}, a turnover number of 2.12 s^{-1} was calculated for 500 s at 0.15 V (vs. SCE) in 1 M glucose.

We performed, in parallel to the electrochemical experiments, XPS measurements to further investigate the stability of (DPDE)Au(III) towards electrocatalytic glucose oxidation, to get more insight in the electrocatalytic behavior of (DPDE)Au(III) and to investigate the formation of Au(0) by electrochemical reduction. The samples were coated on carbon felts and especially prepared without the Nafion® protection layer in order to improve signal capture and avoid overlapping of its XPS signals with those of the matrix.

In a first stage, reference samples MWCNT/(DPDE)Au(III) and MWCNT/(DPDE)H_2 were analyzed. The high resolution (HR) Au4f XPS spectra was studied in order to verify metal insertion into porphyrin and also to extract a reference value for the Au4f peak position for the Au(III) complex (Figure 3A a, b and c). When Au(III) is incorporated into the porphyrin core, the Au4f region (Figure 3A, c) shows two peaks ($Au4f_{7/2}$ and $Au4f_{5/2}$) at 88 eV and 92 eV, which is in accordance with binding energies reported for Au(III) tetraphenylporphyrin (88.4 eV and 91.7 eV)[27].Then, the XPS spectra were recorded for MWCNT/(DPDE)Au(III) after electrocatalysis and after electrochemical reduction of (DPDE)Au(III) at -1.6 V (vs. SCE). The Au4f region (Figure 3A, c and d) shows two peaks which remain unchanged for the MWCNT/(DPDE)Au(III) samples before and after electrocatalytic oxidation of glucose. After electrochemical reduction of (DPDE)Au(III) at -1.6 V (vs. SCE), the binding energies of the Au4f peaks shifted to 84 eV ($Au4f_{7/2}$) and 88 eV ($Au4f_{5/2}$) (Figure 3A, e) confirming the formation of Au(0) corresponding to Au in its zero oxidation degree[27]. These results are in good agreement with the results obtained by cyclic voltammetry. It is important to notice, in that case, Au(0) is expected to be removed from the porphyrinic core.

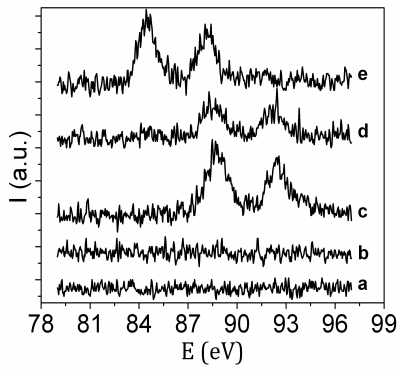

Figure 4. Au4f core levels XPS spectra of (a) MWCNT, (b) MWCNT/(DPDE), (c) MWCNT/(DPDE)Au(III) before glucose electrocatalysis, (d) MWCNT/(DPDE)Au(III) after glucose electrocatalysis and (e) MWCNT/(DPDE)Au(III) after poising the electrode at -1.6 V.

To further investigate the formation of Au(0) via electrochemical reduction of (DPDE)Au(III) at -1.6 V (vs SCE), electron microscopy (SEM and TEM) was used to observe morphological changes. Figure 5A shows a SEM image of the surface of a MWCNT/(DPDE)Au(III) electrode. No aggregates of the porphyrin catalyst were observed. This was confirmed by higher magnification TEM observations of the MWCNT/(DPDE)Au(III) sample. The micrograph in Figure 5D represents the TEM micrograph of this (DPDE)Au(III)/MWCNT sample. Here, a dark shadow around the MWCNTs reveals the presence of a heavy element coating. These shadows are assigned to the (DPDE)Au(III) attached to the MWCNTs, as confirmed by XPS via π-stacking interactions. Interestingly, the contrast along the nanotubes is not homogenous and these shadows are not always visible on the MWCNT. This might be due to a high amount of defects on the outer MWCNT wall preventing stable π–π–interactions. Figure 5B and 5E show SEM and TEM micrographs, respectively, of the surface of a MWCNT/(DPDE)Au(III) electrode after reduction at -1.6 V (vs. SCE). AuNPs appear to be homogeneously distributed within the MWNCT network. The presence of AuNPs demonstrates that the Au(III) ions are expelled from the porphyrin ring during reduction, which is followed by Au(0) aggregation at the surface of MWCNTs. As seen in Figure 5C, energy selective backscattered electron imaging enhances the contrast of AuNPs that appear as white dots. Higher magnification TEM images such as that in Figure 5E clearly show that AuNPs are located on the surface of the MWCNTs. Their diameter was estimated to be between 1 and 5 nm. These characterizations demonstrate the formation of AuNPs via electrochemical reduction of (DPDE)Au(III). These findings shed light on the electrocatalysis results obtained for the reduced form of (DPDE)Au(III) as it allows to explain safely that These AuNPs are involved in the lower-potential oxidation of glucose.

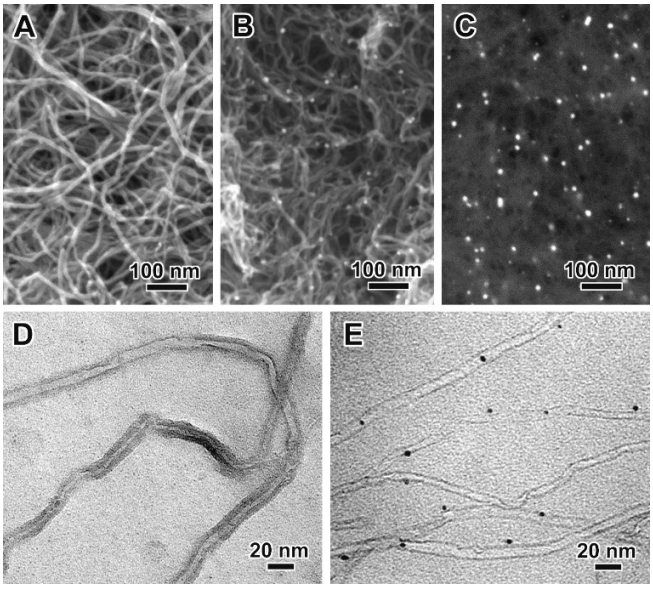

Figure 5. A,B) SEM images (secondary electrons) of a MWCNT/(DPDE)Au(III) electrode and MWCNT/(DPDE)Au(III) after poising the electrode at -1.6 V, respectively. C) same sample as in B imaged with backscattered electrons (EsB). D,E): TEM images of a MWCNT/(DPDE)Au(III) electrode and MWCNT/AuNPs after electrochemical reduction of Au(III) at -1.6 V, respectively.

In conclusion, the electrocatalytic properties of (DPDE)Au(III) towards glucose oxidation in alkaline medium were evaluated. (DPDE)Au(III) exhibits a low onset potential (-0.46 V (vs. SCE)) towards glucose oxidation. This onset potential is 0.185 V (vs. SCE) more positive than Au(0) and 0.33 V (vs. SCE) more positive than Rh(III)porphyrins[9] but still negative compared to those with other complex-based electrocatalysts such as Co macrocycles[28], Ru bipyridine[29] and polymerized Ni porphyrins[30]. Furthermore, we demonstrated the excellent stability of (DPDE)Au(III) towards glucose and its role as a precursor of AuNPs by electrodeposition at low potentials. These promising properties are of great interest in the future design of molecular glucose fuel cells

Acknowledgements

The authors would like to thank the platform "Functionalization of Surfaces and Transduction" of the scientific structure "Nanobio" for providing facilities. The authors also thank the ANR P2N-2010, project GLUCOPAC for financial support. The XPS study presented in this work has been supported by the French National Research Agency (ANR) through the "Recherche Technologique de Base" Program.

Notes and references

[a] Univ. Grenoble Alpes, DCM, F-38000 Grenoble, France.
CNRS, DCM, F-38000 Grenoble, France

[b] Institut Nanosciences et Cryogénie, Laboratoire de Chimie Inorganique et Biologique, UMR E3 CEA UJF, CEA Grenoble, 17 rue des Martyrs, 38054 Grenoble, France

[c] Centre de Recherches sur les Macromolécules Végétales (CERMAV-CNRS), UPR 5301, BP 53, 38041 Grenoble Cedex 9, France – affiliated with Université Joseph Fourier and member of Institut de Chimie Moléculaire de Grenoble and Institut Carnot PolyNat

† Electronic Supplementary Information (ESI) available: [Additional experimental details and characterization data for new compound]. See DOI: 10.1039/b000000x/

1. S. Kerzenmacher, J. Ducrée, R. Zengerle, and F. von Stetten, 2008, 1–17.
2. M. Holzinger, A. Le Goff, and S. Cosnier, *Electrochimica Acta*, 2012, 179–190.
3. P. Kavanagh and D. Leech, *Phys. Chem. Chem. Phys.*, 2013, **15**, 4859–4869.
4. B. Reuillard, A. Le Goff, C. Agnès, M. Holzinger, A. Zebda, C. Gondran, K. Elouarzaki, and S. Cosnier, *Physical Chemistry Chemical Physics*, 2013, 4892–4896.
5. M. Pasta, F. La Mantia, and Y. Cui, *Electrochimica Acta*, 2010, **55**, 5561–5568.
6. C. Baatz and U. Prüße, *Catalysis Today*, 2007, **122**, 325–329.
7. U. Prüße, M. Herrmann, C. Baatz, and N. Decker, *Applied* Catalysis *A: General*, 2011, **406**, 89–93.
8. M. Comotti, C. Della Pina, R. Matarrese, and M. Rossi, Angewandte *Chemie International Edition*, 2004, **43**, 5812–5815.
9. S. Yamazaki, N. Fujiwara, S. Takeda, and K. Yasuda, *Chem. Commun.*, 2010, **46**, 3607–3609.
10. K. Elouarzaki, A. Le Goff, M. Holzinger, J. Thery, and S. Cosnier, *J. Am. Chem. Soc.*, 2012, **134**, 14078–14085.
11. C. T. Lum, Z. F. Yang, H. Y. Li, R. Wai-Yin Sun, S. T. Fan, R. T. P. Poon, M. C. M. Lin, C.-M. Che, and H. F. Kung, *International Journal of Cancer*, 2006, **118**, 1527–1538.
12. Y. Wang, Q.-Y. He, R. W.-Y. Sun, C.-M. Che, and J.-F. Chiu, *Cancer Res*, 2005, **65**, 11553–11564.
13. C.-M. Che, R. W.-Y. Sun, W.-Y. Yu, C.-B. Ko, N. Zhu, and H. Sun, Chem. *Commun.*, 2003, 1718–1719.
14. R. W.-Y. Sun, W.-Y. Yu, H. Sun, and C.-M. Che, *ChemBioChem*, 2004, **5**, 1293–1298.
15. J.-C. Chambron, J.-P. Collin, J.-O. Dalbavie, C. O. Dietrich-Buchecker, V. Heitz, F. Odobel, N. Solladié, and J.-P. Sauvage, *Coordination Chemistry Reviews*, 1998, **178–180, Part 2**, 1299–1312.
16. S. Fukuzumi, K. Ohkubo, W. E, Z. Ou, J. Shao, K. M. Kadish, J. A. Hutchison, K. P. Ghiggino, P. J. Sintic, and M. J. Crossley, *J. Am. Chem. Soc.*, 2003, **125**, 14984–14985.
17. M. P. Eng, T. Ljungdahl, J. Andréasson, J. Mårtensson, and B. Albinsson, *J. Phys. Chem. A*, 2005, **109**, 1776–1784.
18. S. Müllegger, W. Schöfberger, M. Rashidi, L. M. Reith, and R. Koch, *J. Am. Chem. Soc.*, 2009, **131**, 17740–17741.
19. C.-Y. Zhou, P. W. H. Chan, and C.-M. Che, *Org. Lett.*, 2006, **8**, 325–328.
20. K. M. Kadish, W. E, Z. Ou, J. Shao, P. J. Sintic, K. Ohkubo, S. Fukuzumi, and M. J. Crossley, *Chem. Commun.*, 2002, 356–357.
21. Z. Ou, T. Khoury, Y. Fang, W. Zhu, P. J. Sintic, M. J. Crossley, and K. M. Kadish, *Inorg. Chem.*, 2013, **52**, 2474–2483.
22. A. Morozan, S. Campidelli, A. Filoramo, B. Jousselme, and S. Palacin, *Carbon*, 2011, **49**, 4839–4847.
23. A. Le Goff, V. Artero, B. Jousselme, P. D. Tran, N. Guillet, R. Metaye, A. Fihri, S. Palacin, and M. Fontecave, *Science*, 2009, **326**, 1384–1387.
24. C. Leger, S. Dementin, P. Bertrand, M. Rousset, and B. Guigliarelli, *Journal of the American Chemical Society*, 2004, **126**, 12162–12172.
25. C. Engelbrekt, K. H. Sørensen, J. Zhang, A. C. Welinder, P. S. Jensen, and J. Ulstrup, *J. Mater. Chem.*, 2009, **19**, 7839–7847.
26. A. J. Bard and L. R. Faulkner, *Electrochemical methods: fundamentals and applications*, Wiley, second edition., 2001.
27. S. Müllegger, W. Schöfberger, M. Rashidi, T. Lengauer, F. Klappenberger, K. Diller, K. Kara, J. V. Barth, E. Rauls, W. G. Schmidt, and R. Koch, *ACS Nano*, 2011, **5**, 6480–6486.
28. L. M. Santos and R. P. Baldwin, *Anal. Chem.*, 1987, **59**, 1766–1770.
29. E. Villagra, F. Bedioui, T. Nyokong, J. C. Canales, M. Sancy, M. A. Páez, J. Costamagna, and J. H. Zagal, *Electrochimica Acta*, 2008, **53**, 4883–4888.
30. M. do S. M. Quintino, H. Winnischofer, M. Nakamura, K. Araki, H. E. Toma, and L. Angnes, *Analytica Chimica Acta*, 2005, **539**, 215–222.

